Available online at www.sciencedirect.com
SCIENCE DIRECT®
Polymer 45 (2004) 1959–1969
polymer
www.elsevier.com/locate/polymer

Structure evolution in polymer blending using microfabricated samples

Yong Yang[1], L. James Lee[1,*], Kurt W. Koelling[2]

Department of Chemical Engineering, The Ohio State University, Columbus, OH 43210, USA

Received 1 August 2003; received in revised form 18 December 2003; accepted 9 January 2004

Abstract

The transient rheological behavior and morphology evolution of polymethyl methacrylate (PMMA)/polystyrene (PS) binary polymer blends with well-defined initial structure were measured in simple shear flow under isothermal conditions. The size and distribution of the dispersed phase and the composition of the blends were designed and fabricated by Computer Numerical Controlling (CNC) machining, photolithography, and micro-embossing. Compatibilizer can easily be placed at the interface of the two components during sample preparation. The effects of initial dispersed domain size, blend composition, and interfacial tension on rheological behavior and morphology evolution were investigated. It was found that the transient shear stress and first normal stress difference are very sensitive to these parameters. The transient rheological responses up to the breakup point are compared with those predicted by both Doi–Ohta and Vinckier–Moldenaers–Mewis models.

Keywords: Microfabricated polymer blends; Transient rheological behavior; Morphology evolution

1. Introduction

Blending of polymers is an important method to obtain new materials. Since most polymers are immiscible, blending usually leads to a heterogeneous morphology, e.g., a dispersed, stratified, or co-continuous morphology. Blend properties depend on its morphology, which can be tailored to a particular application.

The most commonly used blending method is to mix polymers in an intensive compounder, such as a twin-screw extruder or a high intensity batch mixer. In general, there are four sequential regimes during blending [1–4]. At the start, the polymers exist as elastic solid pellets. At elevated temperatures, pellets become soft and deform under stress. Depending on the transition temperatures and composition, the mixture may go through various transition states, such as forming a co-continuous structure, followed with phase inversion. The final stage is a two-phase viscoelastic fluid. This process is non-isothermal and the flow field in the compounder is often very complicated, making it very difficult to quantitatively investigate the blending process.

To better understand the blending mechanism, many fundamental studies on immiscible blends were carried out in simple flow under isothermal conditions. Taylor [5] performed a pioneering work on a single Newtonian drop in a Newtonian matrix. He pointed out that the deformation of the drop was governed by two dimensionless numbers: the capillary number and the viscosity ratio. Elemans et al. [6] investigated the deformation and breakup of isolated Newtonian drops in a Newtonian matrix. The deformation of a single viscoelastic drop in a viscoelastic matrix and the breakup and coalescence of drops in a viscoelastic matrix have also been studied by many researchers [7–13]. The initial structure was well-defined while the concentration of the dispersed phase was relatively low in these studies.

For highly concentrated blends, several researchers [14–18] have used model blends consisting of Newtonian or nearly Newtonian fluids to study the rheology–morphology relationship in simple shear flow. It was found that, upon a stepwise increase in shear rate, there was a simultaneous occurrence of an undershoot of shear stress, σ_{12}, and an overshoot of the first normal stress

* Corresponding author. Tel.: +1-614-292-2408; fax: +1-614-292-9271.
E-mail addresses: yangy@che.eng.ohio-state.edu (Y. Yang), leelj@che.eng.ohio-state.edu (L.J. Lee), koelling@che.eng.ohio-state.edu (K.W. Koelling).
[1] Tel.: +1-614-292-1216; fax: +1-614-292-3769.
[2] Tel.: +1-614-292-2256; fax: +1-614-292-9271.

0032-3861/$ - see front matter © 2004 Elsevier Ltd. All rights reserved.
doi:10.1016/j.polymer.2004.01.015

difference, N_1, followed by a gradual change to steady state values over a wide range of composition. Takahashi and Noda [16] proposed that the excess shear stress, $\sigma_{12,\text{excess}}$, and the excess first normal stress difference, $N_{1,\text{excess}}$, could be expressed as:

$$\sigma_{12,\text{excess}} \propto \langle n_1 n_2 \rangle \tag{1}$$

$$N_{1,\text{excess}} \propto \langle n_2^2 - n_1^2 \rangle \tag{2}$$

where $\sigma_{12,\text{excess}}$ and $N_{1,\text{excess}}$ are obtained by subtracting the contribution of the polymer components using a linear mixing rule based on volume fraction from the measured σ_{12} and N_1 respectively, $\langle\ \rangle$ is the average on the interface, n is the unit normal vector to the interface, the subscript 1 is the direction parallel to the flow, 2 is perpendicular to the flow direction. In the initial stage of shearing, the dispersed domains are stretched out and form rods, sheets, or fibrils, $\langle n_1 n_2 \rangle$ becomes smaller while $\langle n_2^2 - n_1^2 \rangle$ remains large. As a result, $\sigma_{12,\text{excess}}$ due to interfacial tension becomes small while $N_{1,\text{excess}}$ becomes larger. When the stretched domains break up and retract, $\langle n_1 n_2 \rangle$ increases and $\langle n_2^2 - n_1^2 \rangle$ decreases. This is the reason why the undershoot of σ_{12} and the overshoot of N_1 result from a stepwise increase of shear rate.

Investigations of highly concentrated, non-Newtonian polymer blends also showed the same characteristic transient stress upon stepwise changes in shear rate [19,20]. The initial sample structure was prepared by either steady state shearing at a low rate or randomly mixing solid pellets in a continuous matrix. These methods resulted in a dispersed domain size distribution in the samples, which inevitably affects the accuracy of any quantitative modeling of rheological results during blending, in particular, during start-up experiments. Compared with Newtonian blends, non-Newtonian blends show larger values of $\sigma_{12,\text{excess}}$ and $N_{1,\text{excess}}$, which are due to the contributions of viscoelasticity resulting from both the time evolution of interfacial area and that of the pure polymer components.

Several models have been proposed to predict the transient rheological behavior during blending. Doi and Ohta [14] modeled the transient rheological responses of 1:1 mixtures of immiscible Newtonian fluids with the same viscosity. They derived a semiphenomenological kinetic equation to describe the time evolution of interfacial area (Q) per unit volume and its anisotropy (q_{ij}) in a given flow field. The excess shear stress is proportional to q_{ij}, the steady structure of the distorted interfaces, which is affected by the external flow and the interfacial tension. The external flow orients the interface to an anisotropic state. As a consequence, the interfacial area increases. The interfacial tension has an opposite influence. This model has been found applicable for blends with different compositions [15] and for blends with slightly elastic components [16].

Vinckier and co-workers [18] combined the Doi–Ohta model and the affine deformation theory for a single drop to model the blends with slightly viscoelastic components. They used a linear mixing rule based on the volume fraction for the difference in the component viscosity. The droplet shape is approximated by a cylinder and up to the point where the elongated dispersed phase breaks up. The Vinckier–Moldenaers–Mewis model (VMM model) gives:

$$\sigma_{12} = \left(\sum \Phi_i \eta_i\right)\dot{\gamma} + \frac{2\alpha\Phi\left(1 + \frac{\gamma^2}{2} + \frac{\gamma}{2}\sqrt{\gamma^2+4}\right)^{1/4}}{d_0\sqrt{\gamma^2+4}} \tag{3}$$

$$N_1 = \left(\sum \Phi_i N_{1,i}\right) + \frac{2\gamma\alpha\Phi\left(1 + \frac{\gamma^2}{2} + \frac{\gamma}{2}\sqrt{\gamma^2+4}\right)^{1/4}}{d_0\sqrt{\gamma^2+4}} \tag{4}$$

where $N_{1,i}$ is the first normal stress difference of component i, η_i are the viscosities of the matrix and of the inclusion, Φ_i is the volume composition of component i, Φ is the volume composition of the inclusion, d_0 is the initial dispersed domain size, α is the interfacial tension, $\dot{\gamma}$ is shear rate, and γ is the total strain.

When only considering the affine deformation and neglecting the relaxation terms, the Doi–Ohta model can be simplified as the following equations:

$$\sigma_{12} = \left(\sum \Phi_i \eta_i\right)\dot{\gamma} + \frac{\alpha Q_0 \gamma}{3}\left(1 + \frac{\gamma^2}{3}\right)^{-1/2} \tag{5}$$

$$N_1 = \left(\sum \Phi_i N_{1,i}\right) + \frac{\alpha Q_0 \gamma^2}{3}\left(1 + \frac{\gamma^2}{3}\right)^{-1/2} \tag{6}$$

where the initial specific interfacial area Q_0, which is determined by Φ and d_0, is given as:

$$Q_0 = \frac{6\Phi}{d_0} \tag{7}$$

Both models can qualitatively predict the transient rheological behaviors of Newtonian or near Newtonian blends under shear flow up to the breakup point of inclusions.

Lee and Park [21] extended the Doi–Ohta model to non-Newtonian blends. They took into account the mismatch of viscosities of different polymers by introducing a viscosity ratio term into the equation of stress tensor. In the model they also considered three different types of relaxation: coalescence, shape relaxation and breakup of inclusions by interfacial tension.

Lacroix et al. [20,22] introduced another mixing rule, which considered bulk rheological properties of the components. To further refine governing equation for morphology evolution, the researchers emphasized that the models must incorporate coupling effects between the bulk and interfacial properties. However, the Lee–Park model and modified versions are semiphenomenological, where the initial dispersed domain size was analyzed by morphological observation and one parameter of relaxation terms was obtained by fitting rheological data.

Morphology evolution including phase inversion of polymer blends in steady simple shear flow under

isothermal conditions has been studied by Lazo and Scott [23,24]. They pressed polystyrene (PS) pellets into very thin polyethylene disks. The initial sample morphology was not well-defined and their sample preparation technique was limited to blends where the continuous phase is less viscous than the dispersed phase at the molding temperature. They provided qualitative interpretation of morphology development, but did not report any rheological changes during blending.

Polymer blending is a very complicated process, where the temperature and flow fields are not well-defined, and the concentration of minor phase varies from low, less than 10%, to high, 50%. In the studies of single drop or many drops, the temperature field, flow field, and the initial sample structure are well-defined, but the drop concentration is too low to cause any measurable rheological changes. In the studies of model blends and polymer blends, the temperature and flow fields are again well-defined, and the sample composition is similar to that of actual polymer blends. However, the initial sample structure is not well-defined.

In this paper, highly concentrated polymer blends with well-defined initial structure are prepared using CNC machining, photolithography, and micro-embossing techniques. The transient rheological response and morphology evolution of these microfabricated samples in simple shear flow under isothermal conditions were measured to elucidate the effects of particle size, blend composition, and compatibilizer on rheology change and structure formation.

2. Experimental

2.1. Materials

The materials used in this study include poly(methyl methacrylate) (PMMA), PS, and a di-block polymer: poly(styrene-*b*-methylmethacrylate) (P(S-*b*-MMA)) as a compatibilizer. PMMA (PL-150, $M_n = 105,000$) was donated by Plaskolite Inc. PS (STYRON 685D, $M_n = 120,000$) was donated by Dow Chemical. P(S-*b*-MMA) (P2400-SMMA, $M_n = \text{PS}(46,100) - \text{PMMA}(21,000), M_w/M_n = 1.09$) was supplied by Polymer Source Inc. Fig. 1 shows the steady state shear viscosity as a function of shear rate for PMMA and PS at 200 °C measured by a rheometer (Rheometrics RMS 800) with a cone and plate fixture. The viscosity ratio is 2.16 for the blends of PMMA dispersed in PS at 0.5 s^{-1} and 200 °C. PMMA and PS pellets were dried overnight at 80 °C in a vacuum oven before use.

During sample preparation, a rubbery material (SP 2207), poly(dimethylsiloxane) (PDMS, SYLGARD 184), an epoxy photoresist (Nano SU-8 100), and a propylene glycol methyl ether acetate (PGMEA) developer (Nano XP) were used. SP 2207 is a 80 wt.% ethylene—20 wt.% methyl acrylate random copolymer, donated by Eastman Chemicals. PDMS was supplied by Dow Corning. SU-8 100 and XP Developer were supplied by MicroChem Corp.

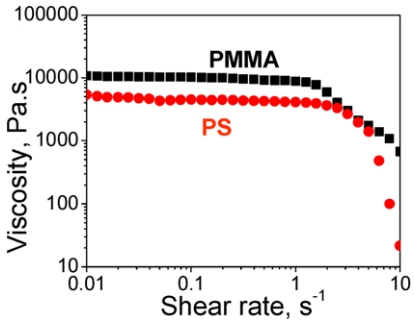

Fig. 1. Viscosity of PMMA and PS as a function of shear rate at 200 °C.

2.2. Preparation of microfabricated samples

The first step in the preparation of microfabricated samples is to make a female PDMS mold, in which wells with pre-specified dimensions are arranged in a hexagonal pattern. If the dispersed domain size in the sample is larger than 100 μm, CNC machining can be used to prepare the master for the mold. We used CNC machining to prepare a female aluminum (Al) mold, where the well size was 1 mm in diameter and 1.5 mm in height with an aspect ratio of 1.5 (aspect ratio is defined as the ratio of feature depth to its width). Followed with hot-embossing at 120 °C and 0.35 MPa, a male SP 2207 rubber mold was made from the Al mold after de-embossing. A mixture of PDMS resin and curing agent with a weight ratio of 10:1 was cast onto the rubber mold. After 4 h curing at 60 °C, the female PDMS mold was peeled off from the rubber mold. We also tried direct casting of PDMS mixture onto a male Al mold. However, de-embossing turned out to be a problem because of the high aspect ratio.

If the domain size is less than 100 μm, photolithography can be applied. Our photolithography process [25] involves photomask fabrication, wafer cleaning, spin coating of the photoresist, soft baking, UV-exposure, post-exposure baking, and developing. In this study, a desired pattern was created with FreeHand (a computer-aided design (CAD) software) and then transferred onto a transparency using a high-resolution laser printer (3386 dpi). On the black background of the photomask, transparent dots with 100 μm in diameter and 50 μm in spacing form a hexagonal array. The fabrication process was carried out as shown in Fig. 2. A silicon wafer was used as the substrate, which was pretreated with isopropyl alcohol, followed by a deionized water rinse, and then dehydration in an oven for 10 min at 120 °C. A thick layer of epoxy photoresist, SU-8 100, was poured onto the substrate and then the substrate was spun with a spin coater (Model P6700, Specially Coating Systems Inc.) to achieve the desired photoresist thickness. After spinning, the substrate was soft baked 10 min at 65 °C and

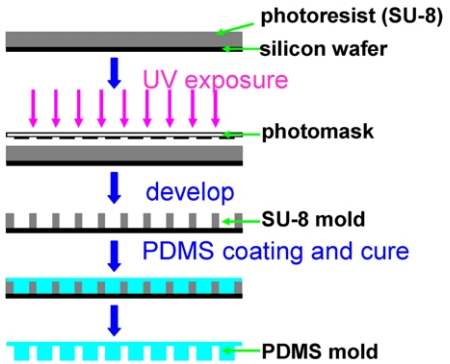

Fig. 2. Schematics of fabricating PDMS mold by photolithography.

then 30 min at 95 °C on leveled hot plates. The exposure was performed on a Cobilt mask aligner with UV light (350–400 nm). The exposure time depends on incident intensity (J/cm^2) or dose. After exposure, the substrate was post-exposure-baked 3 min at 65 °C and then 10 min at 95 °C on leveled hot plates. Subsequently, the substrate was immersed into the SU-8 developer to develop all the features. This produces an SU-8 mold with positive features. Then the mixture of PDMS resin and curing agent was poured onto the male SU-8 mold. After 4 h curing at 60 °C, the female PDMS mold was peeled off from the SU-8 mold.

With the female PDMS mold made from either CNC machining or photolithography, the well-defined samples can be produced by a series of hot-embossing steps. The embossing steps are shown in Fig. 3. Polymer A (PMMA in this study) substrate was isothermally embossed under a constant pressure of 1.0 MPa with the PDMS female mold insert at 230 °C. During embossing, a vacuum was applied to prevent air from re-entering the substrate. Polymer A male mold was obtained after de-embossing at 70 °C. Hot-embossing of polymer B (PS) substrate using the polymer A mold is a non-isothermal embossing process, which means that there is a temperature difference between the mold insert and the polymer substrate. In this process, PS was heated to 210 °C and the cold polymer A mold was then

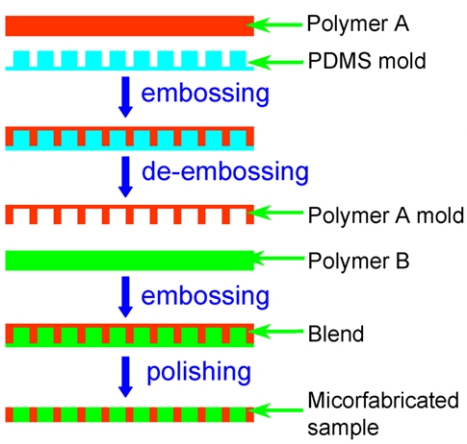

Fig. 3. Schematics of fabricating samples with well-defined initial structure by hot-embossing processes.

embossed onto the molten polymer B substrate. This non-isothermal embossing procedure is necessary because of the close glass transition temperatures between the two polymers. After cooling, a blend of polymer A and polymer B was obtained. The top and bottom layers of the blend were removed by polishing on 20 cm diameter carbide abrasive discs (Leco Corp.) in the following order: 320 grit, 600 grit, 800 grit, and 1200 grit; until the surface of the blend was smooth as observed under a microscope. For each step during sample fabrication, a profilometer (Veeco NT 3300) was utilized to examine part quality. Fig. 4(a) shows a three-dimensional (3-D) plot of the SU-8 mold. The 2-D profile indicates that the feature size is 100 μm in diameter and 150 μm in height as designed. Fig. 4(b) shows the well-defined sample with 100 μm dispersed domains ('100 μm sample' will be used to represent samples with 100 μm diameter dispersed domains through the paper and '1 mm sample' for 1 mm dispersed domains.).

In the case of samples with compatibilizer, a ca. 10 μm thick compatibilizer film (for 1 mm samples) was first spin-coated on the polymer B plate as shown in Fig. 5. The pre-made male polymer A mold was then pressed onto the plate coated with the compatibilizer film by non-isothermal hot-embossing at 210 °C and 1.0 MPa. Again, the sample was polished to remove the top and bottom layers.

Well-defined polymer A particles can be formed in the female mold during embossing. If there is still a thin polymer A layer left, proper solvent (e.g., methylene chloride) can be applied to remove the layer. The formed polymer A particles were removed from PDMS mold by either mechanical force or ultrasonic force and collected. The collected polymer A particles were mixed with fine polymer B powder according to the composition, and the mixture was then molded into a disk shape. In this way, a randomly distributed sample was prepared. Fig. 6 shows a 1 mm randomly distributed sample and a 1 mm well-defined sample.

In this study, six types of samples were prepared as listed in Table 1. In all cases, PS is the initial matrix phase. The samples with 60/40 volume composition of PMMA/PS phase invert during blending. Samples with 40/60 composition of PMMA/PS are for studies of transient rheological behavior only. The dispersed PMMA phase has a diameter of either 1 mm or 100 μm. For comparison, PMMA

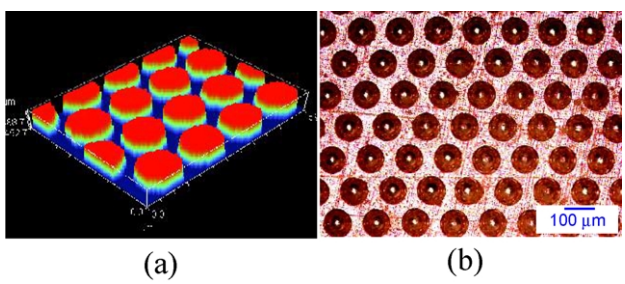

Fig. 4. (a) 3-D plot of the SU-8 male mold, and (b) optical microscopy picture of the 100 μm sample (Sample V).

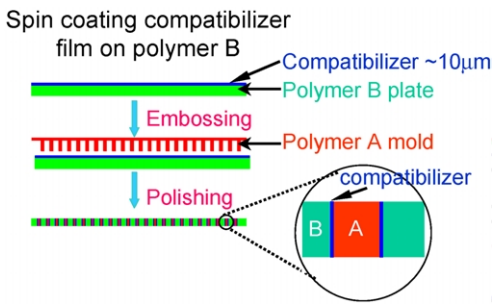

Fig. 5. Schematics of fabricating samples with compatibilizer at the polymer–polymer interface.

Table 1
Summary of samples

Samples	Composition, PMMA/PS	Sample size (mm)		Feature size (μm)		Initial structure
		Diameter	Thickness	Diameter	Height	
I	60/40	25	1.2	1000	1200	Well-defined
II	60/40	25	1.2	1000	1200	Well-defined with compatibilizer
III	60/40	25	1.2	1000	1200	Random
IV	40/60	25	1.2	1000	1200	Well-defined
V	40/60	7.9	0.1	100	100	Well-defined
VI	40/60	7.9	0.1	100	100	Random

particles were also randomly distributed in the PS matrix (Samples III and VI). Before blending, all the samples were dried overnight in a vacuum oven at 80 °C to prevent volatiles from re-entering the samples.

2.3. Blending in a rheometer

A Rheometrics RMS 800 rheometer with a 25 mm parallel plate fixture was used for 1 mm samples, and a 7.9 mm parallel plate fixture for 100 μm samples. First, the sample chamber was gradually heated to 200 °C over 30 min. The 1 mm sample was placed on the bottom plate fixture for another 30 min (in the studies of 100 μm samples three 100 μm thick layers were stacked to form a thicker sample, and the sample was placed on the bottom parallel plate fixture). Then the top parallel plate was slowly moved down until the gap was closed to 1.5 mm (0.35 mm for 100 μm samples). The chamber was opened and the excess polymer was removed from the edge of the plates with a razor blade. The chamber was then closed and the sample was again heated to 200 °C for 10 min. The gap was adjusted to 1.2 mm (0.3 mm for 100 μm samples). After the desired gap was achieved another 10 min waiting time was allowed before starting the blending process. All measurements were carried out at 200 °C under the steady state mode with a constant shear rate of 0.5 rad/s. At the end of measurements, the chamber was opened and dry ice was quickly applied to cool down the sample. At room temperature, the sample could be easily removed from the plates. At least three tests were taken for each set of sample.

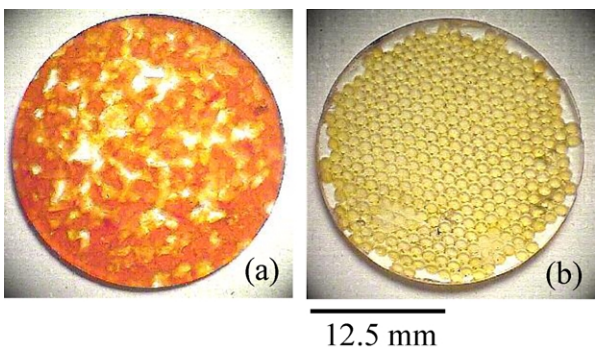

Fig. 6. Photographs of (a) 1 mm randomly distributed sample (Sample III) and (b) 1 mm well-defined sample (Sample I).

2.4. Microscopy measurement

For microscopy observation, all samples were examined at a location 2.5 mm away from the 1 mm sample edge along the flow direction ($r/R = 0.8$). Scanning electronic microscopy (SEM) images were obtained from a Philips XL 30 machine using an accelerating voltage of 12 kV. SEM samples were cryogenically fractured after immersion in liquid nitrogen for 20 min. Then the PS phase was removed with carbon disulfide. The fractured samples were mounted on aluminum stubs and sputter coated with gold. Transmission electron microscopy (TEM) images were with a Reichart Ultracut Ultramicrotome and vapor stained with 4% osmium tetroxide for one hour.

3. Results and discussion

3.1. Transient rheological behavior

Fig. 7 shows the rheological behavior of 1 mm samples (Samples I and III). The first normal stress difference N_1 and the shear stress σ_{12} of both PMMA and PS increase fast and reach the steady state values gradually. At early stage of blending, an overshoot of N_1 and an undershoot of σ_{12} of the well-defined sample (Sample I) were observed. When the dispersed PMMA domains were randomly distributed in the PS matrix (Sample III), no clear N_1 overshoot can be observed and σ_{12} undershoot becomes weaker compared to Sample I. However, when the dispersed domain size was

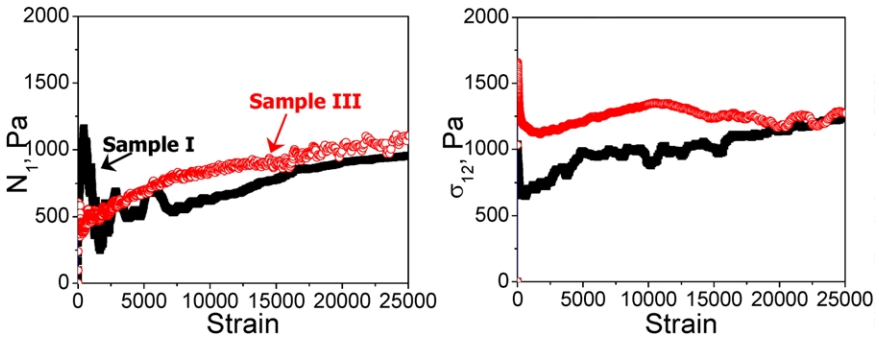

Fig. 7. Rheological responses of 1 mm well-defined and randomly distributed samples (Samples I and III).

reduced from 1 mm to 100 μm, the rheological behavior is different as shown in Fig. 8. The N_1 overshoot and the σ_{12} undershoot can be observed for both the 100 μm well-defined sample (Sample V) and the 100 μm randomly distributed sample (Sample VI). The N_1 overshoot and the σ_{12} undershoot of the well-defined sample are much stronger than those of the randomly distributed sample.

Within the randomly distributed samples, the dispersed particles are not uniformly distributed and oriented, as shown in Fig. 6(a). During steady state shearing the particles experienced a broad range of deformation. As a result, the $N_{1,\text{excess}}$ and $\sigma_{12,\text{excess}}$ due to time evolution of the interfacial area and interfacial tension are small or even negligible like Sample III. For the well-defined sample, the distribution and orientation of dispersed domains are uniform throughout the sample. In simple shear flow, the dispersed domains deformed uniformly. Consequently, the $N_{1,\text{excess}}$ and $\sigma_{12,\text{excess}}$ were much larger.

When the dispersed domain size was reduced from 1 mm to 100 μm, the initial specific interfacial area Q_0 increased from 3600 m^2/m^3 to 24,000 m^2/m^3 for the well-defined samples. Consequently, the N_1 overshoot and σ_{12} undershoot became stronger. It indicates that the transient rheological responses are sensitive to the initial structure of blends.

Using microfabrication techniques we can change one of the blend structure parameters, such as the initial dispersed domain size, blend composition, or interfacial tension, while keep others constant. This allows us to investigate these parameters individually.

When blend composition and interfacial tension are fixed, the effect of the initial dispersed domain size on transient rheological behavior is shown in Fig. 9. For the 100 μm sample (Sample V), the $N_{1,\text{excess}}$ increased linearly until a peak value of 13,500 Pa around a strain of 500, while that of the 1 mm sample (Sample IV) increased to a peak value of 2410 Pa around a strain of 100. At the beginning of blending, the $\sigma_{12,\text{excess}}$ of the 100 μm sample decreased faster than that of the 1 mm sample. These trends can be explained by the increase of interfacial area. When the dispersed domain size decreases from 1 mm to 100 μm at the same composition of 0.4, the initial specific interfacial area Q_0 increases from 2400 m^2/m^3 to 24,000 m^2/m^3, resulting in stronger rheological transient (In this study dispersed domains exist as individual cylinders. When the inclusion composition is fixed, the initial specific interfacial area ratio between the two samples is inversely proportional to the ratio of their diameters according to Eq. (7). At the same composition, this ratio between the 1 mm sample and the 100 μm sample is 10 when neglecting both top and bottom areas of dispersed cylinders. While the ratio is 10.6 when the top and bottom areas are counted.) The steady state values of $N_{1,\text{excess}}$ and $\sigma_{12,\text{excess}}$ are the same for both samples because the only difference between the two blends lies on the initial dispersed domain size while it is the blend composition that determines the steady state values.

Fig. 10 shows the effect of blend composition on transient rheological behavior of blending. When the volume fraction of PMMA increases from 40% (Sample IV) to 60% (Sample I), the $N_{1,\text{excess}}$ increases faster and

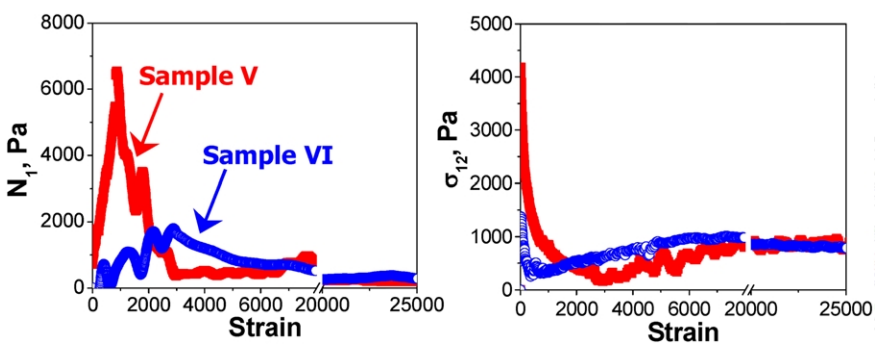

Fig. 8. Rheological responses of 100 μm well-defined and randomly distributed samples (Samples V and VI).

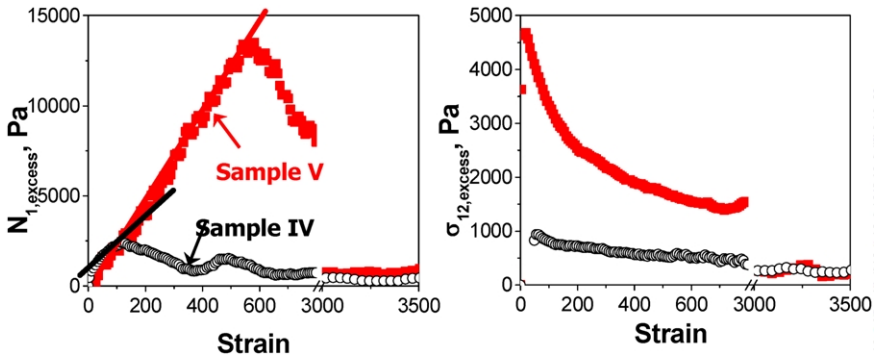

Fig. 9. Effect of dispersed domain size d_0 on transient rheology of microfabricated samples (Samples IV and V).

reaches a higher peak, and the steady state $N_{1,excess}$ is also higher. Sample I also shows stronger $\sigma_{12,excess}$ than Sample IV.

A compatibilizer was added into blends during sample preparation to change the interfacial tension of blends. Fig. 11 shows the effect of adding the compatibilizer on the transient rheological behavior of blending. A sharp N_1 overshoot and an obvious σ_{12} undershoot at early stage of blending for sample without the compatibilizer (Sample I) were observed. However, when the compatibilizer was added (Sample II) the sharp N_1 overshoot disappeared and the σ_{12} undershoot became weaker. The excess rheological responses are determined by the interface area evolution and the interfacial tension. With the compatibilizer, the interfacial area may increase more because of affine deformation, but the interfacial tension became very small. As a result, no clear N_1 peak was observed at the start-up stage for the sample with the compatibilizer.

3.2. Morphology evolution

To further understand what was happening during blending, microscopy observations were made for samples taken from Samples I and II at different strains: 1000, 2000, 9000, 18,000, and 54,000, marked as points **A**, **B**, **C**, **D**, and **E** in Fig. 11. For Point A, SEM observations were carried out as shown in Fig. 12. TEM observations were carried out for rest of the points, from **B** to **E** as shown in Figs. 13 and 14.

At Point **A** (after the N_1 peak), some voids can be observed from Fig. 12(a) for the sample without any compatibilizer. The voids correspond to PS dissolved in carbon disulfide. This indicates that the PS matrix has already broken up. With the compatibilizer, more PMMA sheets were formed as shown in Fig. 12(b), which indicates that the interfacial area increased more with the addition of compatibilizer.

TEM micrographs from the samples without the compatibilizer show the morphology evolution during blending. From Fig. 13 (**B**), a black PS sheet and a white PMMA sheet can be seen. With increasing strain, some holes form in the PS sheets, and the PMMA moves into the holes as shown in Fig. 13 (**C**). Around the interface some PS drops form. Lazo and Scott [23] also observed similar morphology during blending of 85% PS dispersed in a polyethylene matrix in isothermal, steady shear flow. A possible mechanism of PS drop formation is that under stress holes near interface form and are stretched. When the hole wall becomes thin enough the wall breaks up into satellite drops via Rayleigh instabilities. Gradually, more PMMA moves into the PS phase and more PS phase is dispersed in the PMMA matrix as shown in Fig. 13 (**D**). Similar to the description by Scott and coworkers [23], we also found that some PS drops are trapped in the PMMA phase when PMMA sheets coalesce. In other words, 'phase-in-phase' morphology is observed. Finally, the phase inversion is completed where PS is dispersed in the PMMA matrix as shown in Fig. 13 (**E**).

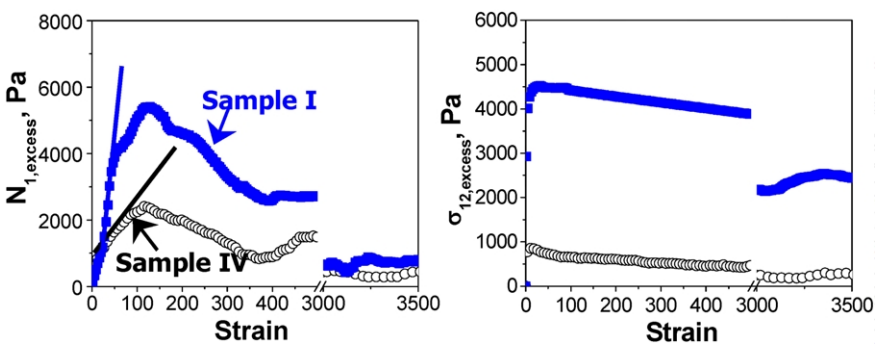

Fig. 10. Effect of composition Φ on transient rheology of microfabricated Samples (Samples I and IV).

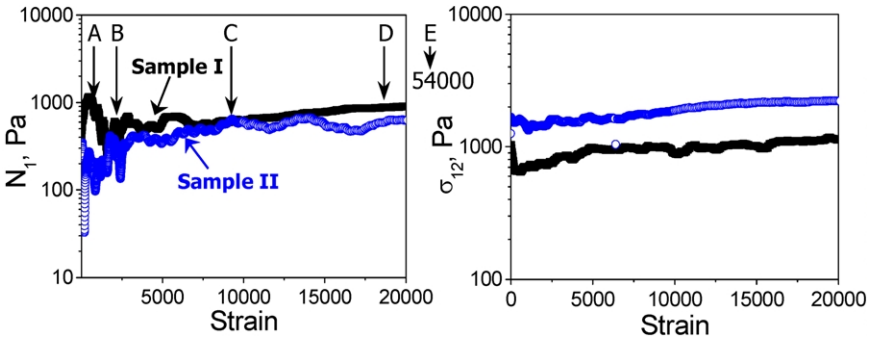

Fig. 11. Effect of interfacial tension α on transient rheology of microfabricated samples (Samples I and II).

With the compatibilizer the morphology evolution is different. Fig. 14 compares the morphology of the samples with and without the compatibilizer at a low and high strain. At the low strain, $\gamma = 9000$, Fig. 14(a) and (c) show that the PS phase has been stretched out more and there are more breakups for the sample with the compatibilizer. Fig. 14(d) shows that the PS phase forms a continuous structure within the PMMA matrix at high strain, while without the compatibilizer PS is dispersed in the PMMA matrix because of phase inversion as shown in Fig. 14(b). In other words, when the compatibilizer is present in the sample, a co-continuous morphology is formed at high strain and no phase inversion is observed.

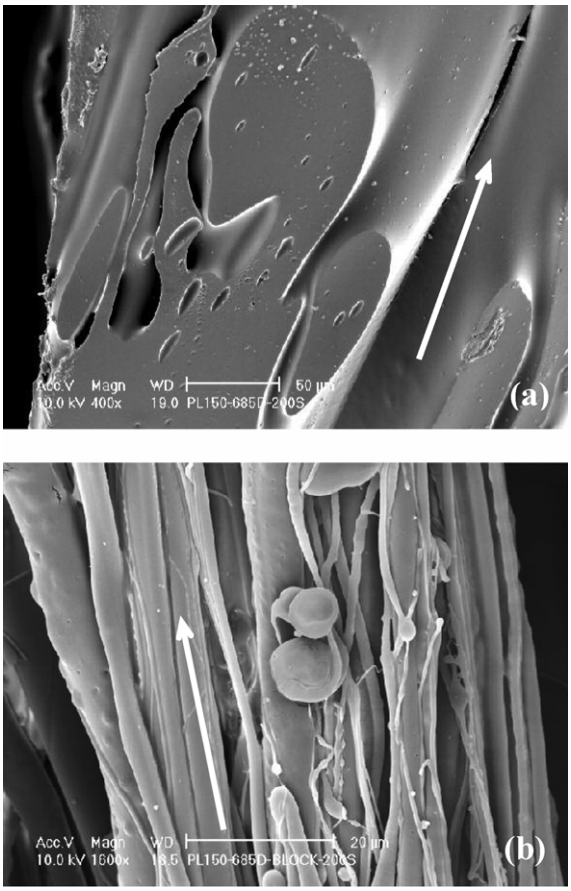

Fig. 12. SEM micrographs of 1 mm well-defined samples (a) without and (b) with the compatibilizer at $\gamma = 1000$. The arrows indicate the flow direction.

This morphological difference can be explained by the difference on interfacial tension. Willemse and co-workers [26] combined the geometrical requirements and micro-rheological conditions to study the stability of extended structures. They proposed the following model:

$$\frac{1}{\phi_{d,cc}} = 1.38 + 0.0213\left(\frac{\eta_m \dot{\gamma}}{\alpha} R_0\right)^{4.2} \tag{8}$$

This model describes the onset composition of co-continuity of a dispersed phase $\phi_{d,cc}$ as a function of the matrix viscosity η_m, interfacial tension α, shear rate $\dot{\gamma}$, and dispersed phase dimension R_0. The model gives the lower limit of the composition range within which a co-continuous structure can exist. The upper limit can be calculated by changing the roles of the two components in the blend. When the compatibilizer is added, the interfacial tension α decreases and the onset composition $\phi_{d,cc}$ also decreases. This means that the co-continuous structure would exist in a broader composition range and phase inversion is less likely to occur.

3.3. Comparison to model predictions

With the well-defined samples, the rheology data can be compared with model prediction. In this study, the viscosity ratio of the PMMA/PS blend is 2.16, and the interfacial tension α of 1.5 mN/m is assumed [12]. The simplified Doi–Ohta model and VMM model can be applied by assuming that the dispersed domain deformation went through affine deformation during blending [18].

According to VMM and simplified Doi–Ohta models, the $N_{1,excess}$ and $\sigma_{12,excess}$ are functions of the initial dispersed domain size d_0, blend composition Φ, interfacial tension α, and the total strain γ. It is found that the ratios of the partial derivative of $N_{1,excess}$ and $\sigma_{12,excess}$ is the same for both VMM model and Doi–Ohta model (refer to Eqs. (A10)–(A12) in Appendix A). The slopes of $N_{1,excess} \sim \gamma$ and $\sigma_{12,excess} \sim \gamma$ curves are taken from the point where the strain is equal to 10 considering the responding time of the rheometer and compared to model prediction.

When the blend composition and the interfacial tension

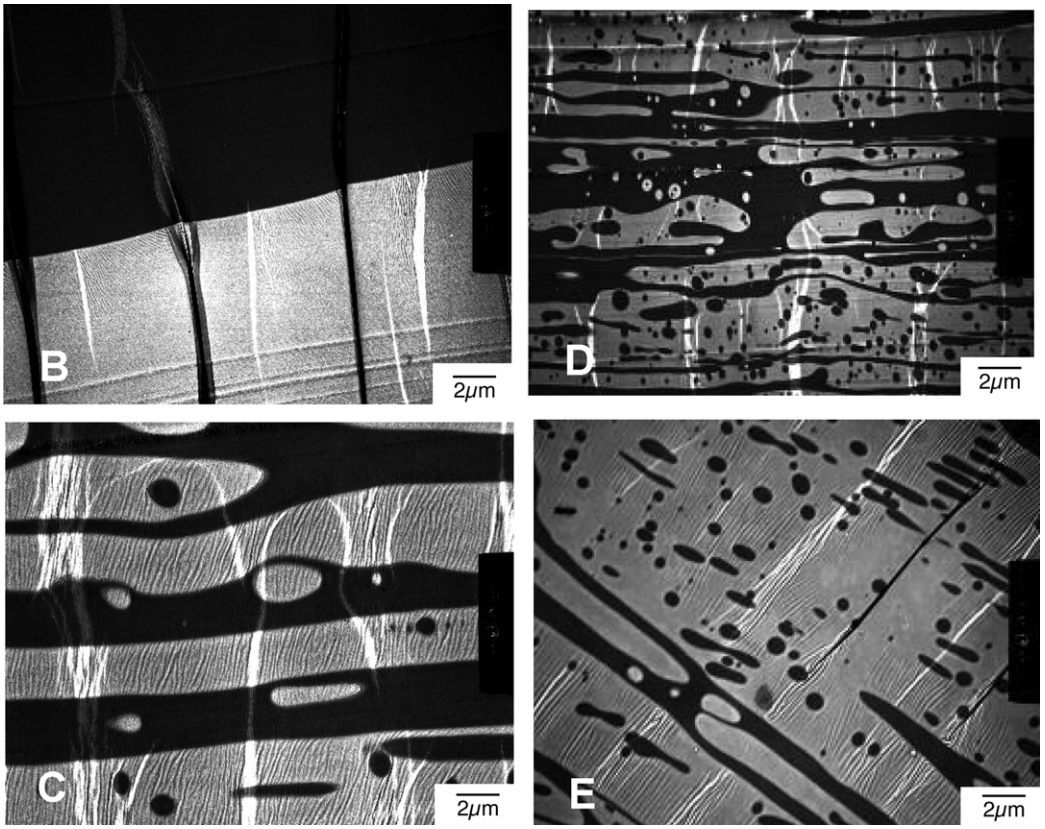

Fig. 13. TEM observations for blends without the compatibilizer at different strains, **B**. $\gamma = 2000$; **C**. $\gamma = 9000$; **D**. $\gamma = 18,000$; **E**. $\gamma = 54,000$.

are fixed and the initial dispersed domain size is decreased from 1 mm to 100 μm, the partial derivative ratios of both $N_{1,\text{excess}}$ and $\sigma_{12,\text{excess}}$ are inversely proportional to the ratio of the initial dispersed domain sizes, i.e., 10. According to Fig. 9, the measured $N_{1,\text{excess}}$ slope ratio is in the range from 4.8 to 5.8, while the $\sigma_{12,\text{excess}}$ slope ratio is in the range from 13.4 to 18.7. When only the blend composition is changed from 40/60 PMMA/PS to 60/40, the partial derivative ratios should be 1.5. The experimental data in Fig. 10 indicate that the $N_{1,\text{excess}}$ slope ratio is from 1.1 to 1.4, while the $\sigma_{12,\text{excess}}$ slope ratio is from 0.9 to 2.4. Since there is no interfacial tension available for Sample II the comparison between model prediction and experimental data cannot be done. However, it can be seen that with the compatibilizer, the interfacial tension is close to zero and $N_{1,\text{excess}}$ is also close to zero. Although the Doi–Ohta model and the VMM model show qualitatively reasonable trends of blending in this study, they are not able to quantitatively predict the transient rheological responses.

4. Conclusion

The blends with well-defined initial structure can be prepared using CNC machining, photolithography, and micro-embossing techniques. Compatibilizer can easily be placed at the interface of polymer blends during microfabrication. With well-defined samples, transient rheological behavior becomes very sensitive to structure changes. Investigations of effects of initial structure, blend composition, and interfacial tension on transient rheological behavior of blending show qualitative agreement with Doi–Ohta model and VMM model. Microfabrication of blends provides a useful tool for quantitative investigation of rheological behavior of polymer blends under well-defined conditions. The presence of compatibilizer strongly affects rheological response during blending and phase inversion, which can be explained by interfacial tension. However, the effects of phase inversion on rheological behaviors of the binary polymer systems were not observed for 1 mm dispersed domain size.

Acknowledgements

We thank Mr Xin Hu for discussion on comparison between the experimental results and modeling. We also want to thank Plaskolite Inc. and Dow Chemical for material donation and National Science Foundation (NSF) sponsored Center for Advanced Polymer and Composite Engineering (CAPCE) at The Ohio State University (CAPCE) for financial support.

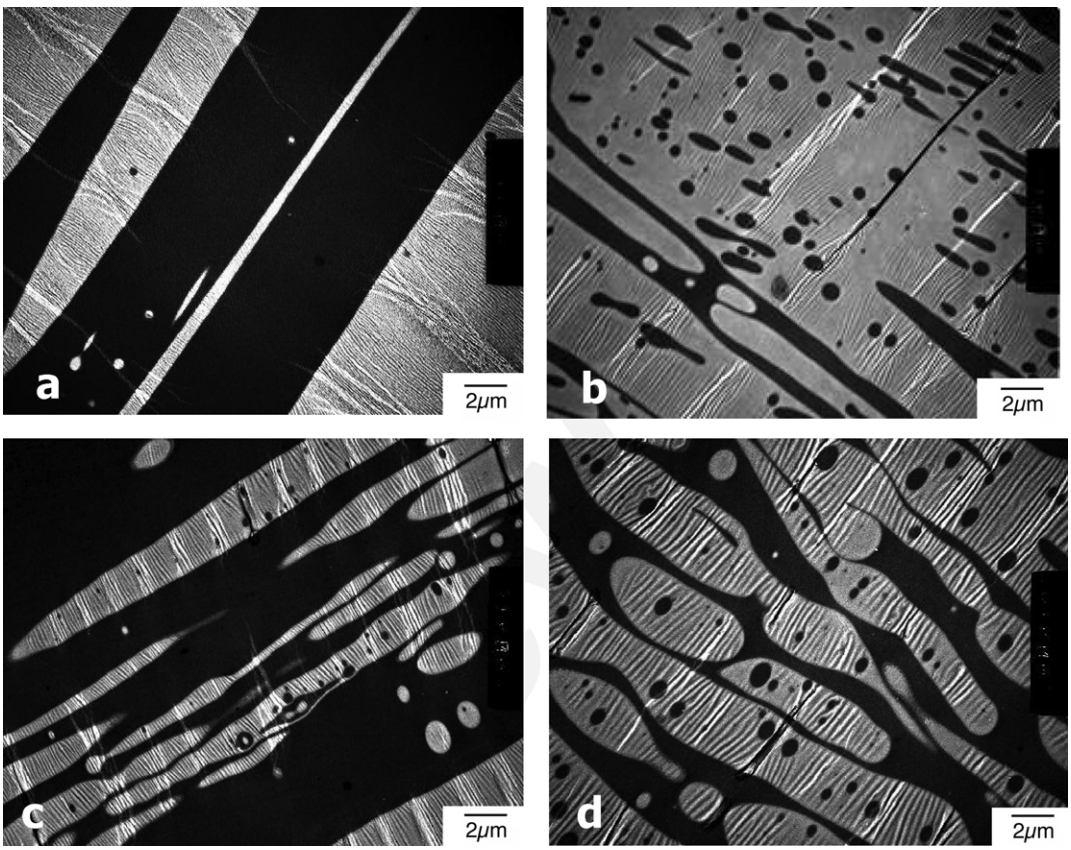

Fig. 14. TEM micrographs of microfabricated samples without the compatibilizer (**a**) $\gamma = 9000$; (**b**) $\gamma = 54,000$ and with the compatibilizer (**c**) $\gamma = 9000$; (**d**) $\gamma = 54,000$.

Appendix A

From Vinckier et al. [18] the shear stress σ_{12} results from the two components and the excess shear stress $\sigma_{12,\text{excess}}$ as shown in Eq. (A1).

$$\sigma_{12}(\gamma, \dot{\gamma}, d_0) = \left(\sum \Phi_i \eta_i\right)\dot{\gamma} + \sigma_{12,\text{excess}} \tag{A1}$$

When combining Eqs. (3) and (A1), and taking partial derivative of $\sigma_{12,\text{excess}}$ with respect to total strain γ, the equation becomes:

$$\frac{\partial \sigma_{12,excess}}{\partial \gamma} = \frac{\partial\left[\sigma_{12} - \left(\sum \Phi_i \eta_i\right)\dot{\gamma}\right]}{\partial \gamma} = \frac{2\alpha\Phi}{d_0} f_1(\gamma) \tag{A2}$$

where

$$f_1(\gamma) = \frac{\left[1 + \frac{\gamma^2}{2} + \frac{\gamma}{2}(\gamma^2+4)^{1/2}\right]}{4(\gamma^2+4)^{1/2}\left[1 + \frac{\gamma^2}{2} + \frac{\gamma}{2}(\gamma^2+4)^{1/2}\right]^{3/4}} \tag{A3}$$

For the excess first normal stress difference $N_{1,\text{excess}}$, the VMM model has the following partial differential form:

$$\frac{\partial N_{1,\text{excess}}}{\partial \gamma} = \frac{\partial\left(N_1 - \sum \Phi_i N_{1,i}\right)}{\partial \gamma} = \frac{2\alpha\Phi}{d_0} f_2(\gamma) \tag{A4}$$

where

$$f_2(\gamma) = \frac{1 + \frac{3\gamma^2}{2} + \gamma(\gamma^2+4)^{1/2} + \frac{\gamma^2}{2}(\gamma^2+4)^{-\frac{1}{4}} - 4\gamma^2(\gamma^2+4)^{-1}\left[1 + \frac{\gamma^2}{2} + \frac{\gamma}{2}(\gamma^2+4)^{1/2}\right]}{4(\gamma^2+4)^{1/2}\left[1 + \frac{\gamma^2}{2} + \frac{\gamma}{2}(\gamma^2+4)^{1/2}\right]^{3/4}} \tag{A5}$$

Following the same procedure, the Doi–Ohta model gives:

$$\frac{\partial \sigma_{12,\text{excess}}}{\partial \gamma} = \frac{2\alpha\Phi}{d_0} f_3(\gamma) \tag{A6}$$

where

$$f_3(\gamma) = \frac{3}{3+\gamma^2}\left(1+\frac{\gamma^2}{3}\right)^{-\frac{1}{2}} \tag{A7}$$

$$\frac{\partial N_{1,\text{excess}}}{\partial \gamma} = \frac{2\alpha\Phi}{d_0} f_4(\gamma) \tag{A8}$$

where

$$f_4(\gamma) = \gamma\frac{6+\gamma^2}{3+\gamma^2}\left(1+\frac{\gamma^2}{3}\right)^{-\frac{1}{2}} \tag{A9}$$

It can be seen that, for both VMM model and Doi–Ohta model, the partial derivatives of $\sigma_{12,\text{excess}}$ and $N_{1,\text{excess}}$ are functions of blends composition Φ, initial dispersed domain size d_0, interfacial tension α, and total strain γ.

If two of three factors, Φ, d_0, and α, are fixed, the effect of the third factor on transient rheological behavior of blending at the same total strain can be investigated. For blends with different compositions but the same initial dispersed domain size d_0 and interfacial tension α, the partial derivative ratio is independent of the total strain as shown in Eq. (A10). In other words, the ratio of the partial derivative of $\sigma_{12,\text{excess}}$ and $N_{1,\text{excess}}$ is the function of blend composition only. In the same way, roles of the initial dispersed domain size and interfacial tension during blending can also be compared as shown in Eqs. (A11) and (A12). In Eqs. (A10)–(A12) subscripts 1, 2 stand for two different samples.

$$\left.\frac{\left(\frac{\partial N_{1,\text{excess}}}{\partial\gamma}\right)_1}{\left(\frac{\partial N_{1,\text{excess}}}{\partial\gamma}\right)_2}\right|_{d_0,\alpha} = \left.\frac{\left(\frac{\partial \sigma_{12,\text{excess}}}{\partial\gamma}\right)_1}{\left(\frac{\partial \sigma_{12,\text{excess}}}{\partial\gamma}\right)_2}\right|_{d_0,\alpha} = \frac{(\Phi)_1}{(\Phi)_2} \tag{A10}$$

$$\left.\frac{\left(\frac{\partial N_{1,\text{excess}}}{\partial\gamma}\right)_1}{\left(\frac{\partial N_{1,\text{excess}}}{\partial\gamma}\right)_2}\right|_{\Phi,\alpha} = \left.\frac{\left(\frac{\partial \sigma_{12,\text{excess}}}{\partial\gamma}\right)_1}{\left(\frac{\partial \sigma_{12,\text{excess}}}{\partial\gamma}\right)_2}\right|_{\Phi,\alpha} = \frac{(d_0)_2}{(d_0)_1} \tag{A11}$$

$$\left.\frac{\left(\frac{\partial N_{1,\text{excess}}}{\partial\gamma}\right)_1}{\left(\frac{\partial N_{1,\text{excess}}}{\partial\gamma}\right)_2}\right|_{d_0,\Phi} = \left.\frac{\left(\frac{\partial \sigma_{12,\text{excess}}}{\partial\gamma}\right)_1}{\left(\frac{\partial \sigma_{12,\text{excess}}}{\partial\gamma}\right)_2}\right|_{d_0,\Phi} = \frac{(\alpha)_1}{(\alpha)_2} \tag{A12}$$

References

[1] Shih CK. Proc SPE ANTEC 1991;49:99–104.
[2] Shih CK. Adv Polym Technol 1992;11(3):223–6.
[3] Shih CK. Polym Engng Sci 1995;35(21):1688–94.
[4] Sundararj U, Macosko CW, Shih CK. Polym Engng Sci 1996;36(13): 1769–81.
[5] Taylor GI. Proc R Soc London A 1934;146:501–23.
[6] Elemans EHM, Bos JH, Jassen JMH, Meijer HEH. Chem Engng Sci 1993;48(2):267–76.
[7] Stone HA, Leal LG. J Fluid Mech 1990;211:123–56.
[8] Fortelný I, Živnỳ A, Juza J. J Polym Sci Part B Polym Phys 1999;37: 181–7.
[9] Fortelný I, Živnỳ A. Macromol Symp 2000;149:157–63.
[10] Börschig C, Fries B, Gronski W, Weis C, Friedrich C. Polymer 2000; 41:3029–35.
[11] Sundararaj U, Dori Y, Macosko CW. Polymer 1995;36(10):1957–68.
[12] Sundararaj U, Macosko CW. Macromolecules 1995;28(8):2647–57.
[13] Levitt L, Macosko CW. Macromolecules 1999;32(12):6270–7.
[14] Doi M, Ohta T. J Chem Phys 1991;95(2):1242–8.
[15] Takahashi Y, Kurashima N, Noda I. J Rheol 1994;38(3):699–712.
[16] Takahashi Y, Noda I. In: Nakatani AI, Dadmun MD, editors. Flow-induced structure in polymers. Washington, DC: ACS; 1995. p. 140–52.
[17] Vinckier I, Moldenaers P, Mewis J. J Rheol 1996;40(4):613–31.
[18] Vinckier I, Moldenaers P, Mewis J. J Rheol 1997;41(3):705–18.
[19] Guenther GK, Baird DG. J Rheol 1996;40(1):1–20.
[20] Lacroix C, Grmela M, Carreau PJ. J Rheol 1998;42(1):41–62.
[21] Lee HM, Park OO. J Rheol 1994;38(5):1405–25.
[22] Lacroix C, Aressy M, Carreau PJ. Rheol Acta 1997;36:416–28.
[23] Lazo ND, Scott CE. Polymer 1999;40:5469–78.
[24] Lazo ND, Scott CE. Polymer 2001;42:4219–31.
[25] Yu L, Koh CG, Lee LJ, Koelling KW. Polym Engng Sci 2002;42(5): 871–88.
[26] Willemse RC, Posthuma de Boer A, van Dam J, Gotsis AD. Polymer 1998;39(24):5879–87.